

INTERGRANULAR CORROSION AND RESIDUAL STRESS DETERMINATION OF A DUPLEX STAINLESS STEEL PIPELINE GIRTH WELD

B Gideon¹, L P Ward²

¹ARV Offshore, Bangkok, Thailand

**²School of Civil Environmental and Chemical Engineering, RMIT University,
Australia**

SUMMARY

Welding of duplex stainless steel (DSS) pipeline material for the oil and gas industry is now common practice. To date research has been conducted primarily on the parent material and heat affected zones in terms of its susceptibility to various forms of corrosion and effects of addition of alloying elements. However there has been little research conducted on the corrosion characteristics and structural transformation of the weld metal in terms of the susceptibility to Intergranular Corrosion (IGC) of the various successive weld layers namely the root, fill and cap layers.

The focus of this paper is to provide an in-depth analysis of residual stress levels within the various regions / phases of duplex stainless steel girth welds and any correlation with susceptibility to IGC. Test methods used to assess the susceptibility to IGC, were ASTM A262 and a modified double loop electrochemical potentiokinetic reactivation (DL-EPR) test. Residual stress levels were determined using a Time of Flight (TOF) neutron diffraction technique. Neutron diffraction was performed at Los Alamos Nuclear Science Centre (LANSCE).

Results obtained from residual stress measurements by neutron diffraction revealed that in the hoop direction, ferrite (211) and austenite (311) exhibits tensile strains in the weld. As the distance from the weld centreline increases out to the heat affected zone (HAZ), an inversion occurs where strains in both the ferrite and austenite are slightly more compressive. In the axial and radial direction, the strains for both phases are more compressive, due to constraint impeding contraction of the weld bead during cooling, and it is likely that this is the dominating effect.

The DL-ERP test results revealed that both the fill layer regions and the base material showed the highest values for Ir/Ia and Qr/Qa. A correlation could not be observed between the strain distribution in the DSS weld regions and the degree of susceptibility to IGC.

KEY WORDS

Duplex Stainless Steel, Intergranular Corrosion, Neutron Diffraction, Electrochemical Potentiodynamic Reactivation, Time of Flight, Heat Affected Zone

1. INTRODUCTION

DSS are used increasingly as an alternative to austenitic stainless steels, especially in chloride or sulphide environments, e.g., in the oil, gas and petrochemical industries (1). In the welding of DSS, it is essential to maintain a ferrite–austenite ratio close to 50:50. This phase balance, may however, be upset due to rapid cooling resulting in weld metal ferrite contents in excess of 50%. In order to restore the phase balance, weld filler materials are usually overalloyed with Ni than in the base material (2). The resultant phase ratio is dependent on the energy input during welding, as this determines the cooling rate and the extent of the phase transformation which is diffusion based.

It has been reported (3,4) that various intermetallic phases (χ , σ and R) can be present in the weld metal under different aging conditions. These phases are predominantly associated with slow cooling rates through specific temperature regions from 600°C to 1000°C (5). It has been shown that the effect of intermetallic phases on the majority of the weld metal properties are only be significant at approximately 2 % volume (5). Secondary austenite (γ') has also been identified in the reheated weld beads of DSS. The corrosion resistances in these welds are reduced due to the lower Mo, Cr, and N contents in austenite, and as a result, welds containing γ' have poorer corrosion resistance (6). One way to limit the formation of γ' in the weld region is to reduce the heat input in the successive passes. This will reduce the reheating and cooling cyclic effect on the structure of the root pass, which will also be in contact with corrosive liquids in the pipeline. Nilsson et al. (6) determined that the as-welded microstructure was almost devoid of intermetallic phases, but small amounts of γ' was present. This observation was based on multipass welds with heat inputs of either 0.8 kJ or 1.4 kJ and interpass temperatures not exceeding 100°C.

Heat input and interpass temperature are the two main welding parameters often cited as influencing the cooling rate. It has been determined that increasing the heat input increases the width of the HAZ (7), while the use of high heat input reducing the corrosion resistance has also been reported (8). A simulated multipass weld was developed to show that the toughness of the HAZ exhibited a maximum when the interpass temperature was maintained below 100°C. In addition, it was established that the toughness of the HAZ increased with an increase in cooling rate (9). It has also been demonstrated that as the interpass temperature increases, the cooling rate decreases (10).

Numerous papers have been published on the microstructures of duplex stainless steel weld metal and HAZs, but detailed studies of the as-welded structures and their susceptibility to sensitization are limited.

The aim of this study is to conduct a detailed analysis of the various weld sections within a DSS pipeline, as a function of heat input and type of weld, in terms of the metallurgical structure, composition and mechanical properties and to assess the susceptibility to IGC.

2. EXPERIMENTAL

2.1. Welding Conditions and Mechanical Testing.

The parent material chosen for the investigation was a 10mm wall thickness, 250mm diameter DSS pipeline corresponding to UNS S31803. The filler material used was the conventional ER2209 AWS A5.9-93 classification. Full details of the chemical composition of both the parent material and filler material are listed in Table 1, confirming that the primary solidification mode was ferrite.

		C	Mn	P	S	Si	Ni	Cr	Mo	N	Cu	Pren	Cr _{eq}	Ni _{eq}
Pipe	Min	-	-	-	-	-	5.00	21.50	3.00	0.15	-	35	-	-
	Max	0.030	2.0	0.025	0.015	1.0	6.50	23.00	5.50	0.20	0.16	-	32.04	10.78
Filler Material	Max	0.016	1.69	-	-	0.42	8.60	23.07	3.20	0.160	0.16	≥35	28.09	11.90

Note; $Cr_{eq} = Cr + 1.37Mo + 1.5Si + 2Nb + 3Ti$ and $Ni_{eq} = Ni + 22C + 0.31Mn + 14.2N + Cu$

Table 1. Chemical composition of pipe and filler material.

Welding was performed using the manual Gas Tungsten Arc Welding (GTAW) technique on a double bevel single U joint configuration. Details are given in Table 2. Radiography (X-ray) was performed to ensure the integrity of the girth welds.

Weld			
Weld Condition	Pass	Travel Speed	Heat Input
		mm/min	J/min
GTAW U groove	1 (weld root)	110.00	419.78
	2 (weld fill)	62.00	757.55
	3 (weld fill)	38.00	1733.05
	4 (weld fill)	40.00	2194.80
	5 (weld cap)	43.00	2041.67
	Average		1429.37

Table 2 Weld Conditions

Ferrite content was determined metallographically by the point count method (11). Vickers hardness measurements were made with a 10 kg load in the parent material, HAZ, weld cap, weld fill and weld root regions. Charpy impact tests were performed to assess the notch toughness of samples extracted from the weldments as described in ASTM A 370 (12). The volume fraction V_f of ferrite was determined from the ASTM E562 point count method.

2.2. Intergranular Corrosion tests (IGC)

Two test methods namely a modified ASTM A262 (13) and a modified Double Loop Electrochemical Potentiokinetic Reactivation (DL-ERP) test were employed to determine the susceptibility to IGC.

Modified ASTM A262 Standard Practices E—copper–copper sulfate, sulfuric acid test for detecting susceptibility to intergranular attack was used. The specimen was covered with copper shot and grindings and immersed in a solution of 16 wt% sulfuric acid with 6 wt% copper sulfate. The solution was then heated to its boiling point and maintained at this temperature for 48 hours. On removal from solution, the specimen was bent through 180° over a rod with a diameter equivalent to twice the thickness of the specimen instead of four times the thickness to ensure if cracks appeared they would be more apparent. The bent surface of the specimen was then examined for cracks at low magnifications in the range X5 to X20.

A modified double loop test was used as conducted by Schultz et al (14-16) as described in Fig.1. The solution used was 0.5M H_2SO_4 + 0.001M TA (thioacetamide). TA was added to reduce the extent of ferrite dissolution. The test was conducted at 60°C. The polarization scan was started 5 minutes after immersion of the specimen. The potential was scanned from -500 mV (SCE) to +200 mV (SCE) and back to -500 mV (SCE) at a rate of 1.67 mV/s. The ratio of the reactivation charge to the passivation charge was calculated and is shown in the results and discussion section.

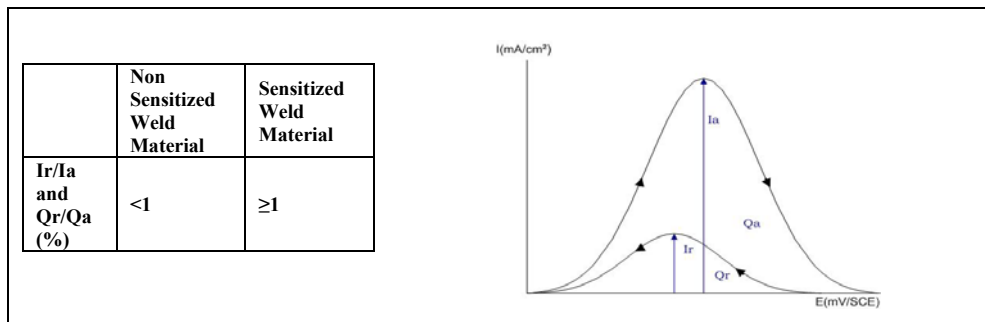


Figure 1. Principle of DL-ERP on Degree of Sensitization (DOS) (17).

Although the EPR test is well established for austenitic stainless steels and has been used for DSS (18-20) the test parameters are dependent on surface preparation and material quality.

Samples for DL-ERP tests were cut from areas as close as possible to where macro sections were taken, for metallographic examinations and hardness measurements. Specimens were cut along the centreline of the welds to allow for an exposed area of 1cm² required for the DL-ERP tests and to reveal the relevant weld layers (Root, Fill and Cap).

2.3 Residual Stress Measurements

Residual strain measurements using a spallation source were made using neutron diffraction at the Los Alamos Nuclear Science Centre (LANSCE). This was to substantiate previous work done at the Australian Strain Scanner at Lucas Heights (24). Residual strains in the ferrite and austenite phases were measured at the locations indicated in Figure 1. Strains were measured in the three directions - longitudinal, transverse and normal (L,T and N) to the welding direction.

LANSCE provides a pulsed neutron source where the neutrons are generated by accelerating protons in a linear accelerator and bombarding them into a Tungsten target. Every time a proton pulse hits the target a burst of neutrons is generated by spallation. Each pulse of neutrons contains a spectrum of wavelengths and is moderated by passing through a chilled water moderator at 10 °C. The incident flight path is 31 meters, most of it in a neutron guide. This instrument has two detector banks at plus and minus 90 degrees to the incident beam with a diffracted flight path length of about 1.5 m, The total flight path, the scattering geometry and the 20 Hz repetition rate of the source dictates that the useable wavelength range to be about 0.4 to 3.8 Å with maximum intensity between 0.5 to 1.5 Å.

The diffractometer was configured for strain scanning with a small incident neutron beam and radial collimators of horizontal width 2 mm in the diffracted beam. The cross-section of the incident beam was defined by computer-controlled boron nitride apertures which were 2 mm wide and 25 mm high for the measurement of the transverse and normal strains and 2 mm high for the measurement of the longitudinal. Two banks of He3 detectors centred at 90° each spanning 10° in the horizontal plane and 15° in the vertical plane, viewed the gauge volume through the radial collimators. The sample was placed on an XYZθ stage with a setting precision of 0.05 mm in the three directions and 0.1° in angle.

The sample was positioned optically with the aid of two Leica™ theodolites that, by triangulation, could locate a point on the surface of the sample with an accuracy of 0.1 mm. The point of interest could then be positioned in the gauge volume with the required direction along the bisector of the incident and diffracted beams by driving the stage.

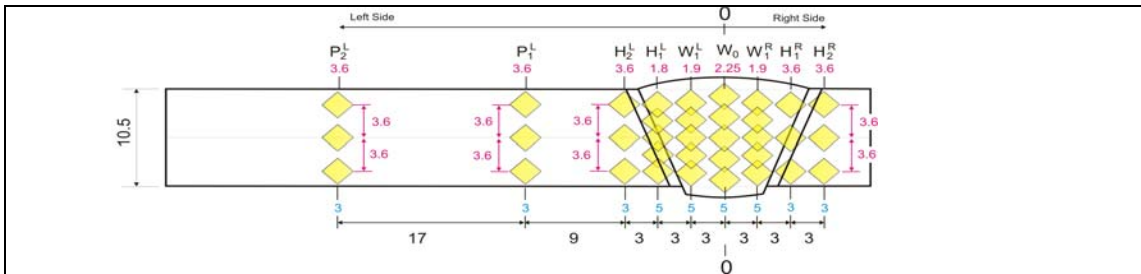


Figure 2 Schematic drawing of neutron diffraction measurement locations in the welds studied

The measurement of residual elastic strain by monochromatic neutron diffraction relies on the use of Bragg's law to relate the lattice spacings, d_{hkl} , to the angle of diffraction $2\theta_{hkl}$ associated with the diffraction peak labelled by Miller indices hkl at a fixed wavelength. Strain was calculated from the selected planar atomic spacing for ferrite and austenite at discrete locations in the weldment using Eq. 1.

$$\varepsilon_{hkl} = (d_{hkl} - d_{hkl}^0) / d_{hkl}^0 \quad \text{Equation 1}$$

The calculation of the residual strains requires the knowledge of an appropriate reference lattice spacing d_{hkl}^0 . This is problematic in welds where there is a possibility of redistribution of alloying elements, and secondly, inhomogeneous plastic deformation across the weld will generate relatively strong intergranular stresses in DSS. This problem was addressed by cutting a companion slice 2mm thick from the weld and cutting slits every 2mm across it's length in order to relieve the

macroscopic residual stress field. Thus, the reference measurements d_{hkl}^0 represented the lattice spacing as a function of position relative to the weld centre and included any effects of alloy diffusion and intergranular stresses.

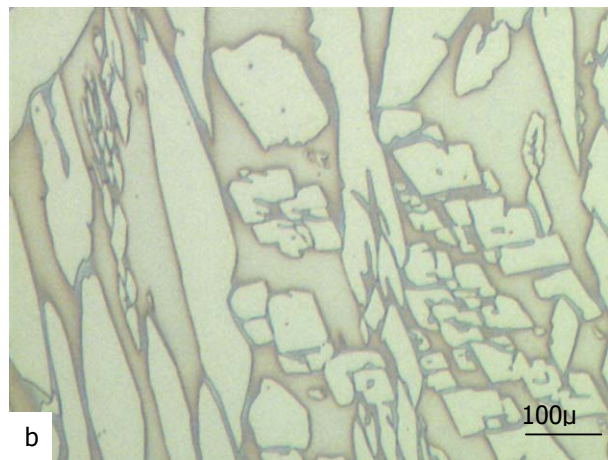
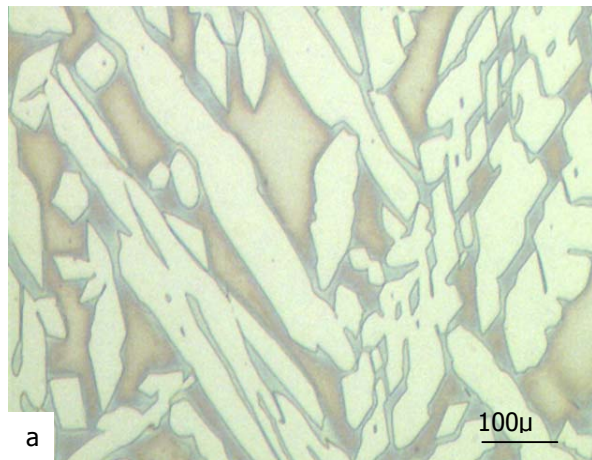
DSS polycrystalline aggregates are known to exhibit both elastic and plastic anisotropy, which results in intergranular residual stresses and texture as a consequence of the thermo-mechanical processing route. The superposition of intergranular residual stresses can lead to errors in measurement of the macroscopic stress field. In this case, the ferrite and austenite lattice spacings were measured using the 211 and 311 diffraction peaks respectively. These hkl values have been observed to behave independently of the intergranular stresses in a similar duplex alloy (23).

3. RESULTS AND DISCUSSION

The microstructure, resulting phase transformation, mechanical properties and degree of susceptibility to IGC are discussed in detail in this section. Microstructural characterization was performed using optical metallography, macrohardness and energy dispersive X-ray spectroscopy (EDS). Table 3 summarises the results of the mechanical properties of the welded duplex stainless steels carried out in this study, while Fig. 2 shows optical micrographs of the welded regions according to the various welding conditions, as indicated in Table 3.

Weld Condition	Weld Pass	Charpy Impact Test	Ferrite determination	Modified ASTM A262 (E)	Modified DL-ERP Test	
		(-43°C)	Point Count		Qr/Qa	Ir/Ia
		J	%			
GTAW	1 (weld root)	97	42.58	Pass	0.05	0.08
	2 (weld fill)		-		-	-
U groove	3 (weld fill)		36.95		0.10	0.12
	4 (weld fill)		-		-	-
	5 (weld cap)		40.03		0.03	0.06
Average					39.85	

Table 3 Summary of the results of the mechanical properties of the welded duplex stainless steels.



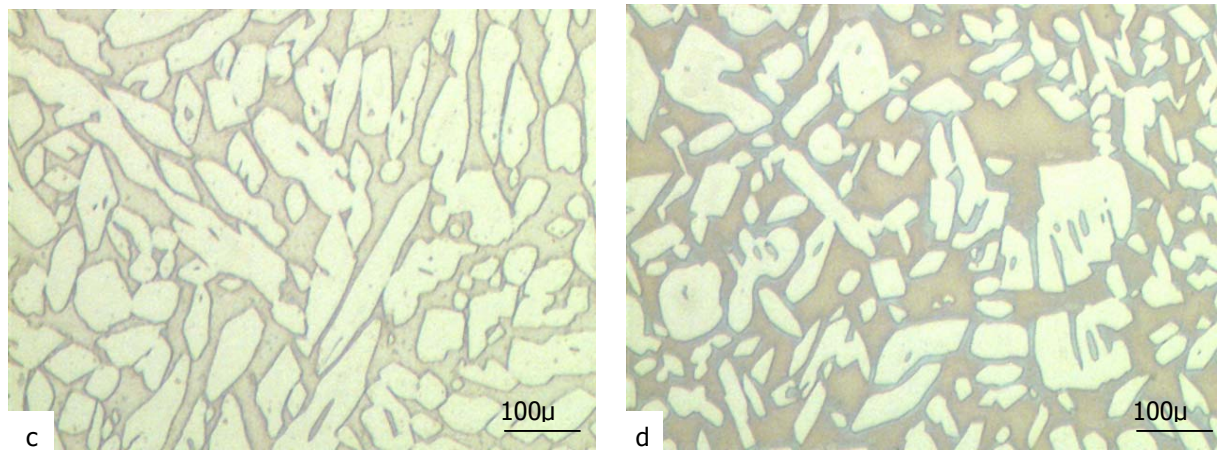


Figure 3: Optical micrographs of the duplex stainless steel weld mechanically polished in successive finer grades of emery papers, from 120 grit to 600 grit. The final polish was a diamond paste (finish of 1 micron) on a polishing cloth and etched in NaOH 0.1M solution with an applied voltage of 1.6 V for 20-25 s.; a) Cap, b) Fill, c) Root region - transverse d) Root region – internal

3.1. Microstructural Evaluation

Microstructural analysis for all four GTAW shown by the optical micrographs in Fig 3 reveals the presence of a two-phase banded structure, typical of such materials. In general, the austenite regions observed in the DSS weld metal is formed from ferrite in three modes, viz., as allotriomorphs at the prior-ferrite grain boundaries, as Widmanstätten side-plates growing into the grains from these allotriomorphs and as intragranular precipitates. In the micrographs, the grain boundary allotriomorphs and Widmanstätten austenite are clearly seen. However, the austenite seen within the grain could be either intragranular precipitates or Widmanstätten austenite intercepted transverse to the long axis. Fig. 3a shows that the grain boundary austenite layer is not continuous. It is further known that the formation of grain boundary and side-plate fractions requires a relatively smaller driving force (18) and therefore can occur at higher temperatures with little undercooling. The formation of intragranular acicular ferrite, on the other hand, requires a greater degree of undercooling and therefore occurs at lower transformation temperatures. It is likely that a similar transformation sequence is adopted during the microstructural evolution of the regions associated with the DSS weld. Thus the grain boundary austenite and Widmanstätten side-plates form early at higher temperatures, while the intragranular austenite particles require a greater driving force and precipitate later at a lower temperature.

Figure 4 shows the distribution of ferrite in and around the weld region and a correlation with analysis of residual stress.

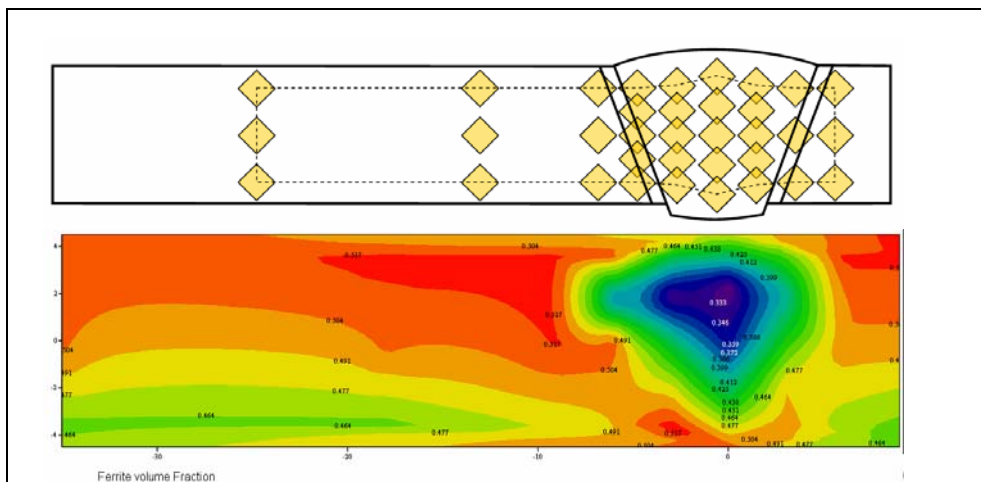


Fig. 4 Distribution of ferrite and measurement locations in the welds studied by neutron diffraction.

3.2. Intergranular Corrosion Tests

The results for the modified A262 Standard Practice E test for all conditions were found to be acceptable, with no intermetallic phases observed during metallographic examination. Such findings can also be substantiated by the high impact energy values obtained (97-116 joules). No evidence of sensitization could be observed in all four weld conditions even under a restricted and reduced bending radius. The results of these findings and details of testing procedure have been discussed elsewhere (22)

3.3. Modified DL-ERP Test

The sensitivity of the DSS welds was evaluated using the DL-EPR test, which consisted of subjecting the weld regions to potentiokinetic scanning in a solution of 0.5M H₂SO₄ + 0.001M TA (thioacetamide), from an active to a passive domain (activation scan), followed by a return to the initial potential (reactivation scan). The test efficiency was measured by means of a response test, which was characterized by weak values of the current density ratio ($I_r/I_a < 1\%$) and the charge ratio ($Q_r/Q_a < 1\%$) for non-sensitized materials, and relatively high ratio values ($I_r/I_a \geq 1\%$) and ($Q_r/Q_a \geq 1\%$) for high-sensitized materials. The reverse polarization from the passive to the active region gave rise to a reactivation peak, the magnitude of which is sensitive to the degree of alloy element depletion. The susceptibility to corrosion was characterized in terms of both the ratio of the reactivation-current peak to the activation current peak as well as the ratio of the reactivation charge to the activation charge (20). Both I_r/I_a and Q_r/Q_a results are represented graphically in Fig. 6. Analysis of the results shows that the fill region for all four weld conditions had a higher degree of sensitization (DOS) compared to the root and cap region of the welds. It was also observed that collectively, condition 4 had the highest DOS for the root and cap region. Typical DL-ERP scans are shown in Fig. 7

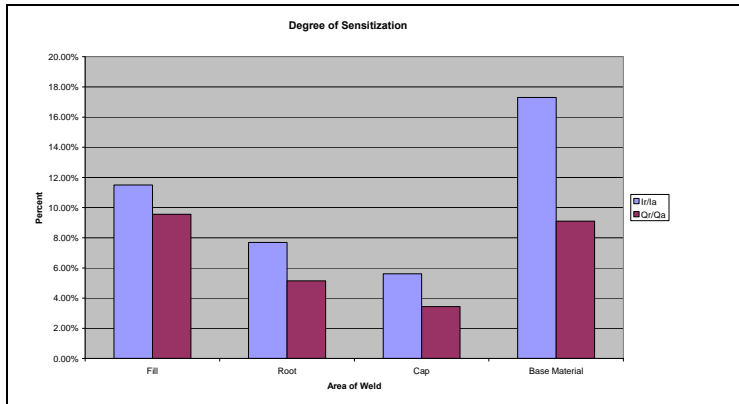


Fig. 5. Results of DL-ERP test showing DOS for all conditions in terms of Q_r/Q_a and I_r/I_a .

The I_r/I_a and Q_r/Q_a results were then compared to the percent of Ferrite transformed in each layer (Root, Fill and Cap). A correlation was observed between the I_r/I_a and Q_r/Q_a values and the amount of ferrite, whereby higher I_r/I_a and Q_r/Q_a values were accompanied by lower ferrite concentrations and lower I_r/I_a and Q_r/Q_a values were accompanied by higher ferrite concentrations, as observed in Fig. 6.

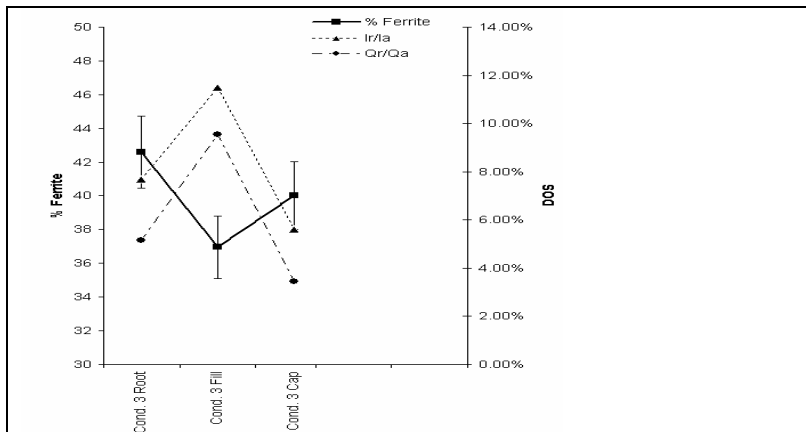


Fig. 6. Correlation of Qr/Qa, Ir/Ia, DOS and %ferrite in all Conditions.

The results of this study confirm the usefulness of the DL-EPR method in evaluating quantitatively the sensitization of DSS in accordance with previous studies (14-16). The DL-EPR method has the advantage of being a fast and quantitative test that can easily be incorporated into the monitoring of equipment to identify, in particular, IGC (20).

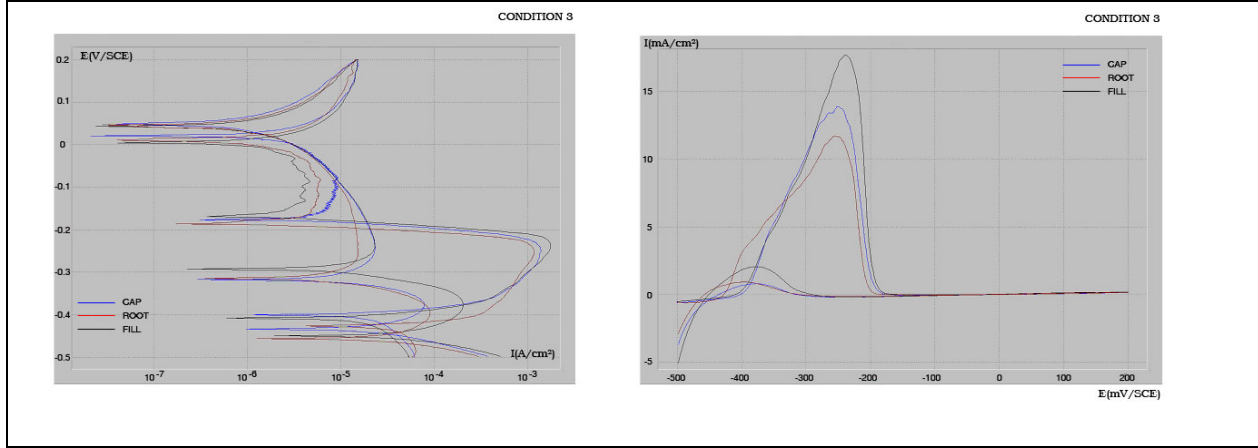


Figure 7 a) Anodic Polarization curve of Root, Fill and Cap region in Condition 3, 0.5M H₂SO₄ + 0.001 M TA. b) DL-ERP plot of Root, Fill and Cap region in Condition 3 showing difference in DOS in 0.5M H₂SO₄ + 0.001 M TA

3.4 Residual Stress Measurement

Residual phase strains averaged over the diffracting volume (2x2x4mm³) in the hoop, axial and radial directions. In two phase or duplex materials, the grains have different physical and elastic properties. Therefore the micro-stresses over the one phase does not equal to zero. In order to calculate the stresses, the following equation (21) was used

applies:

$$\bar{\sigma}_{ij}^{ph} = \bar{\sigma}_{ij}^I + \sigma_{ij}^{phE} + \sigma_{ij}^{phTh} + \sigma_{ij}^{phPl} \quad \text{Equation 2}$$

Where I is the macro-stress, and misfit elastic thermal and plastic stresses are denoted by E , Th and Pl , respectively.

The mismatch stresses are defined as the average value of the micro-stresses over all grains belonging to one phase and for both phases the sum of macro-stresses must be zero over a large volume of material. This can be expressed as:

$$\sigma_{ij}^I = f\sigma_{ij}^{ph1} + (1-f)\sigma_{ij}^{ph2} \quad \text{Equation 3}$$

The summation of the two macro-stresses for both phases is the overall macro-stress.

Since the momentum of a neutron is equal to $h\lambda$

$$\lambda = \frac{ht}{ml} = (2d \sin \theta)_{hkl} \longrightarrow t = \frac{(2mLd \sin \theta)_{hkl}}{h} \quad \text{Equation 4}$$

h is the Planck's constant, m is the neutron mass, L is the flight path of the neutron and t is the travel time of the neutron. All reflections are collected at two fixed scattering angles which are at 90⁰ and -90⁰ from the diffraction spectrum. This is aided by radial collimators between the detector and the sample. These results are expressed in Fig. 8 and 9.

In the hoop direction, ferrite (211) and austenite (311) exhibit tensile strains in the weld. As the distance from the weld centerline increases out to the HAZ (~5mm), an inversion occurs where strains in both the ferrite and austenite are slightly more compressive. In the axial and radial direction, the strains for both phases are more compressive, due to constraint impeding contraction of the weld bead during cooling, and it is likely that this is the dominating effect. Moving out from the weld, the HAZ and base material can be clearly distinguished from the weld as both average phase strains become uniformly tensile.

The stress state of the weld may be affected by elastic mismatch stress, thermal misfits, plastic misfit stresses due to differing plastic behaviour between phases as well as transformation stresses. All of these factors apply locally, due to the multi-pass welding operation, but also to the initial stress state of the pipe from the thermo-mechanical processing history. Overriding all this, long-range residual stresses from the welding process make an interpretation of the short-range phase stresses extremely difficult.

In order to convert phase strain to stress (Eq.2) the diffraction elastic constants E_{hkl} and ν_{hkl} for each phase must be known, and these in turn depend on the crystallographic texture of the weldment which varies with position from parent to weld. Given the demanding experimental requirement for the texture at each location in the weld, a best approximation of the diffraction elastic constants was chosen using the self-consistent scheme proposed by Kröner (23) for random texture. Such that, $E_{211}^\alpha = 225.5$, $E_{311}^\gamma = 183.5$ GPa, and $\nu_{211}^\alpha = 0.28$, $\nu_{311}^\gamma = 0.31$ for the ferrite and austenite phases. The calculated phase and macro stresses (Eq.3 and 4) are shown in Figure 8 and 9.

In the radial direction, the root section of the weld is strongly tensile for austenite and slightly compressive for ferrite. These results may suggest that these regions could be susceptible to cracking.

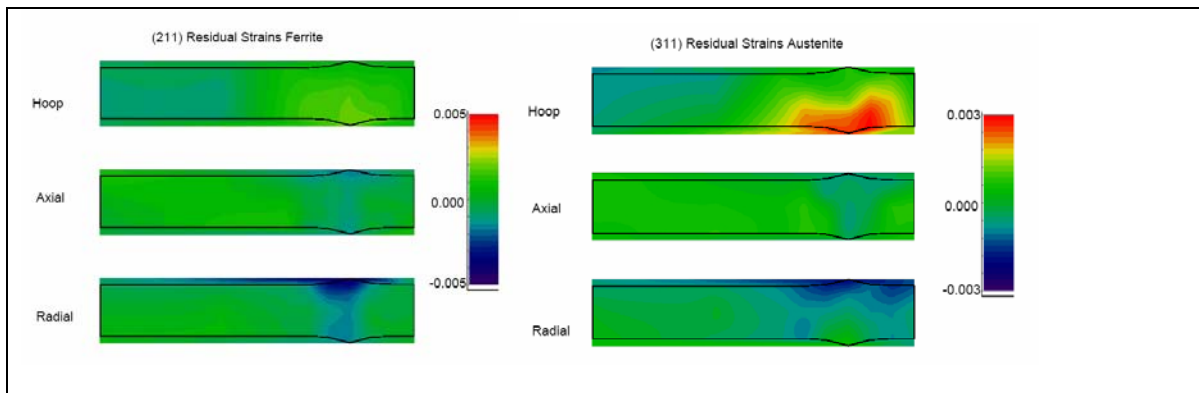
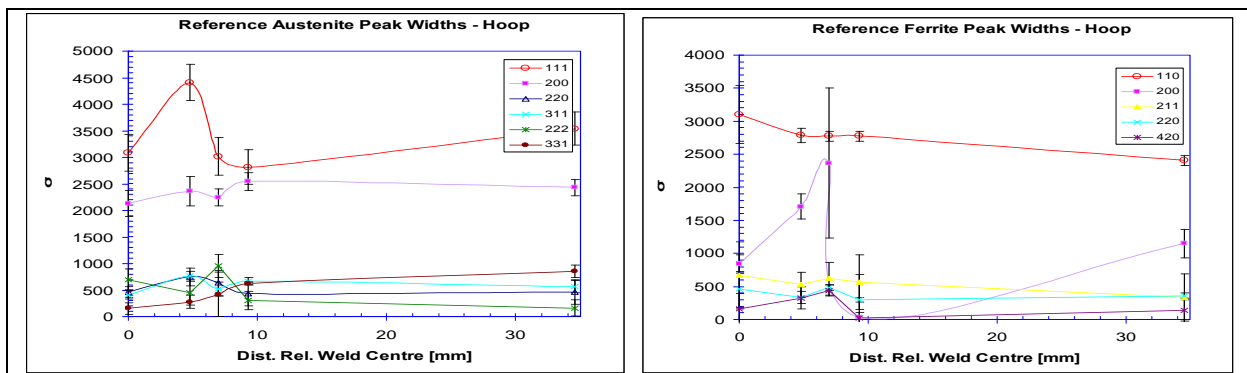


Figure 8. strain distribution in ferrite (211) and austenite (311) as a function of hoop, axial and radial strain distribution in the sample.



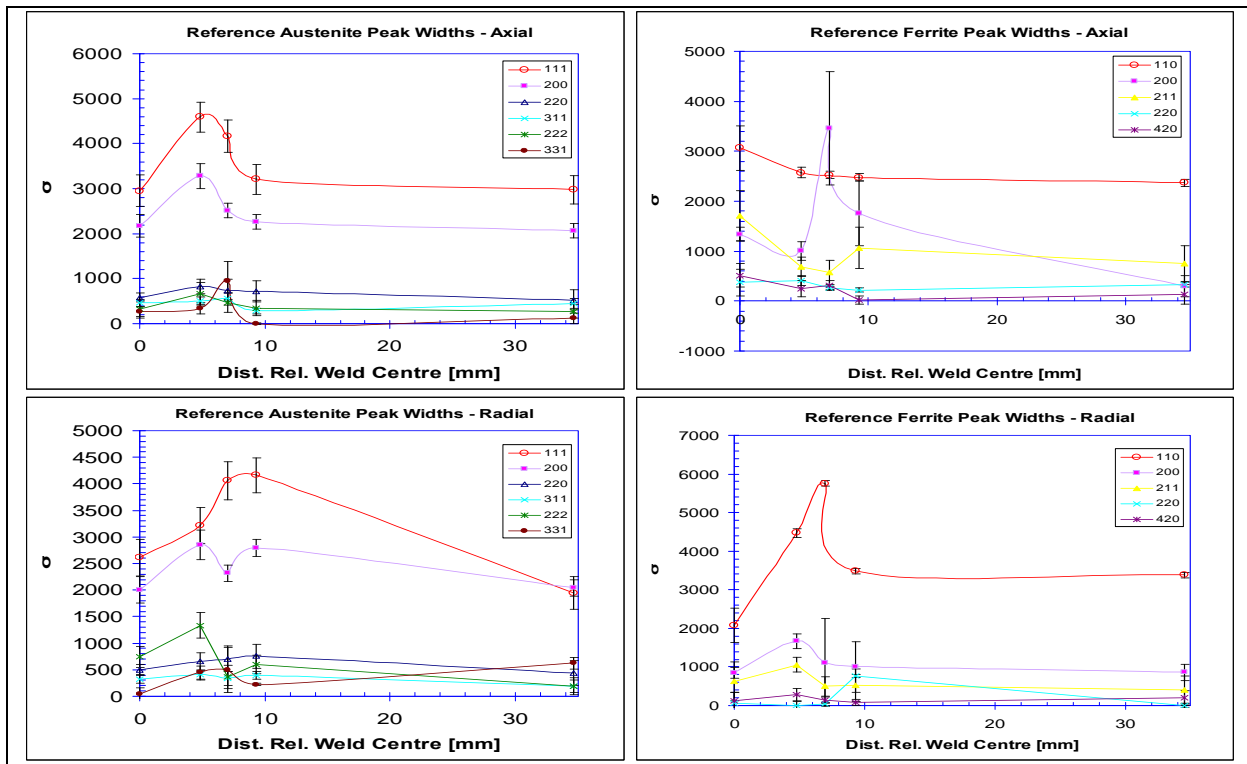


Fig. 9. Distribution of various peak widths

The stress-free lattice spacing is another critical factor in determining the accuracy of strains in measurements performed. Another important aspect is the determination of line shape of the peak as a function of time. It is based on Gaussian function graphically expressed as a sharp leading edge and a lagging tail. Resolution of peaks formed from TOF source is independent of neutron wavelength therefore FWHM of all peaks in a spectrum are the same. FWHM expressed as d-spacings Δd is obtained by the differential equation;

$$\Delta\lambda = \Delta t = \Delta d = \frac{\Delta h}{2mL \sin \theta} \quad \text{Equation 5}$$

This shows that measurements at high detector angles in single scan with high resolutions for various (hkl) reflections is possible since peaks obtained can be resolved. This is dependent on the scattering angle for the specific d-spacing and the flight path L .

4. CONCLUSIONS

- The optical microstructure of the weld metal as detailed in Fig. 1 shows a formation of a finer and coarse structure within the weld metal. This is dependent on the level of undercooling which would be expected in a welding process, since the weld metal in the cap region would cool down more quickly as a result of the lower ambient temperature of the weld surface and adjacent parent material at the start of welding. There was no evidence of secondary austenite (γ'), being present in any of the weld metal conditions examined. In addition, no areas were observed to contain any of the normally expected intermetallic phases or carbides, even at higher magnifications (X 80 000 times) used in the present study.
- There was a significant correlation between the Ir/Ia and Qr/Qa values and the % transformation of Ferrite.
- The DL-ERP test results revealed that the fill area and the base material had the highest values for Ir/Ia and Qr/Qa.
- No correlation could be shown between the Ir/Ia and Qr/Qa and the strain distribution in the weld region.

5. ACKNOWLEDGEMENTS

The Authors wish to acknowledge, D G Carr & Dr. O Muransky from Australian Nuclear Science and Technology Organization (ANSTO), Australia and Dr. Lim Ching Liang from Metacos Malaysia.

6. REFERENCES

1. B D Craig, Sour Gas Design Consideration, SPE Monograph No. 15, (1993).
2. M Liljas, Proc. Fourth International Conference on Duplex Stainless Steels, Glasgow, Scotland, Keynote Paper V, vol. 2, pp13–16 Nov (1994)
3. L Karlsson, L Ryen and S. Pak: Weld , 74, pp28-40 (1995)
4. A Radjarviia, G Metur and M. Gantois: Proc. Conf. Duplex Stainless Steels '91, Beaune, France, , Societe Frangaise de Metallurgie et de Mat6riaux, pp119-126 October (1991)
5. L. Karlsson: Proc. Conf. Duplex Stainless Steels '97, Maastricht, The Netherlands, October 1997; Stainl. Steel World, , pp43-58 (1997)
6. J-O Nilsson, L Karlsson, and J-O Andersson: Mater. SCL. Technol., 11 (3), pp276-283 (1995)
7. S Jana: 'Innovation stainless steel', Florence, Associazione Italiana di Metallurgia, pp3343-3348; (1993)
8. S Atamert and J E King: Acta. Metall, , 39, pp273-285 (1991)
9. H J Yu: Proc 4th Int. Conf. on Trends in Welding Research, , Materials Park, OH, ASM International, pp87-92 (1995)
10. N A McPherson, Y Li and T N Baker, Science and Technology of Welding Journal, 5 (4), pp235-244 (2000)
11. ASTM E562, Standard Test Method for Determining Volume Fraction by Systematic Manual Point Count
12. ASTM A370, Standard Test Methods and Definitions for Mechanical Testing of Steel Products
13. ASTM A262, Standard Practices for Detecting Susceptibility to Intergranular Attack in Austenitic Stainless Steels
14. S Schultze, J Gollner, K Eick, P Veit and I Garz, " The modified EPR test: A new tool for examination of corrosion susceptibility of duplex stainless steel", Duplex '97, Paper D97-067, KCI Publishing, Zutphen, The Netherlands, pp639. (1997)
15. A Turnbull, P E Francis, A J Griffiths, E Bennett, W Nimmo, "Measurement of Corrosion Resistance of Super-Duplex Stainless Steel Welds by Electrochemical Techniques," Eurocorr" 2000, London, U.K. Institute of Materials, (2000).
16. E Otero, C Merino, C Fosca, P Fernandez, "Electrochemical Characterization of Secondary Phases in a Duplex Stainless Steel by EPR Test," Duplex '94, paper no. 56, Cambridge, U.K.: TWI, (1994)
17. B Gideon, L Ward, G Biddle, " Testing and Characterization of Duplex Stainless Steel Welds and their Susceptibility to Intergranular Corrosion", Eurocorr'06, Maastricht, Netherlands, September (2006)
18. B J Ginn and T G Gooch: 'Effect of Intermetallic Content on Pitting Resistance of Ferritic-Austenitic Stainless Steels', proc. conf. Stainless Steels'91 Science and market, Chia Laguna Sardinia, Italy, 3 pp81-89 (1999)
19. L Karlsson: 'Intermetallic Phase Precipitation in Duplex Stainless Steels and Weld Metals: Metallurgy, Influence on Properties and Testing Aspects', Welding in the World, 43, (5) (1999)
20. T Amadou, C Braham, and H Sidhom; Metallurgical and Materials Transactions A 35A, pp3499 (004)
21. T W Clyne and P J Whitters, an Introduction to Metal Matrix Composites, Cambridge Solid State Science Series, Cambridge University Press, Cambridge (1993)
22. B Gideon, L Ward, K Short, Characterization of the Weld Regions within Duplex Stainless Steels using Magnetic Force Microscopy, Journal of Minerals and Materials Engineering Characterization, 7 (3) pp247 - 263 (2008)
23. E Kröner, Berechnung der elastischen konstanten des vielkristalls aus den konstanten des einkristalls, Z. Physik. 151, pp404-418 (1958)
24. B Gideon, L Ward, D G Carr "Strain Measurements by Neutron Diffraction and Characterization of Duplex Stainless Steel Welds" Duplex 2007 Conference, Aquileia and Grado Italy, paper 49 (2007)